MXene alloy-based metal-semiconductor contact for low-resistive field-effect transistors

Check for updates

Saheb Bera, Deepanshu Kaushik & Hemant Kumar ✉

MXenes offer a unique platform for designing high-performance electronic devices due to their diverse properties and chemical tunability. This study focuses on engineering low-resistance metal-semiconductor contacts using MXenes for future field-effect transistor applications. Through a comprehensive approach combining first-principles calculations, transport simulations, and alloy phase engineering, we demonstrate the feasibility of achieving low-resistance contacts with high current-carrying capacity. Through first-principles calculations, we identify promising MXene heterojunctions based on lattice matching and Schottky barrier height. Notably, the Ta_2CO_2-Ti_2CO_2 contact exhibits a remarkably low Schottky barrier height. Using non-equilibrium Green's function calculations, we demonstrate high output current in this contact, indicating low resistance. Further analysis reveals the critical role of carrier density and detrimental impact of metal-induced gap states. To suppress metal-induced gap states, we propose an interfacial alloying strategy using a $Ta_{2x}Ti_{2(1-x)}CO_2$ solid solution, which reduces interfacial charge transfer and promotes smoother electronic coupling. This, in turn, reduces the Fermi-level pinning effect and contributes to a substantial reduction in contact resistance across the MXene interface. This study highlights the potential of MXenes as building blocks for advanced electronics and provides a pathway for engineering high-performance contacts through a combined computational and design approach.

The miniaturization in electronics has pushed silicon-based metal-oxide-semiconductor field-effect transistors (MOSFETs) to their physical limits, leading to the exploration of alternative materials[1]. Two-dimensional (2D) semiconductors have emerged as promising candidates due to their unique electronic properties, atomic-scale thickness, and potential for ultimate scalability[2–4]. These materials can overcome the limitations of conventional silicon technology, including enhanced electrostatic control, high carrier mobility, and tunable bandgaps. However, a major obstacle in developing high-performance electronic devices with 2D semiconductors is the difficulty in forming efficient electrical contacts with metal electrodes. This interface presents unique challenges stemming from the atomic-scale thickness of 2D materials, which can lead to considerable performance limitations. Firstly, the limited contact area inherent to 2D materials results in high contact resistance, impeding efficient charge carrier injection and extraction. This resistance directly affects the device's on-current, transconductance, and overall switching speed. Secondly, Fermi-level pinning at the metal-semiconductor interface can create a Schottky barrier, further hindering charge transport.

Minimizing these detrimental effects requires a multi-pronged approach. Edge contact engineering, where contacts are formed at the edges of the 2D material, can effectively increase the contact area and reduce resistance. Phase engineering of the 2D material in the contact region can favourably modify its electronic properties and promote better energy level alignment with the metal, reducing the Schottky barrier height. Furthermore, judicious selection of contact metals with appropriate work functions is crucial to minimize Fermi level pinning and achieve ohmic contact behavior. Recent efforts in advancing FET technology have focused on utilizing 2D materials, such as germanane, GeSe, phosphorene, and transition metal dichalcogenides (TMDs), as semiconducting channels[5–9]. However, the integration of these 2D semiconductors with conventional 3D metal contacts often results in high contact resistance, primarily due to large Schottky barriers and Fermi level pinning induced by interface dangling bonds, which hinders their performance in high-efficiency FET applications[10–13]. While phase engineering of TMDs, such as MoS_2, offers a potential route to mitigate these issues by creating 2D-2D metal-semiconductor edge contacts, the long-term stability of the metallic phase remains a challenge[14].

School of Basic Sciences, Indian Institute of Technology Bhubaneswar, Argul, Odisha, India. ✉e-mail: hemant@iitbbs.ac.in

In this context, MXenes, a diverse family of 2D transition metal carbides, nitrides, and carbonitrides, present a compelling alternative. Their high electronic conductivity, diverse compositions, and tunable electronic properties make them promising candidates for realizing low-resistive contacts in 2D FETs[15–20]. For example, MXenes based on Group IV transition metals (Ti, Zr, Hf) are metallic in their pristine form but convert to semiconductors when terminated with oxygen[21]. Furthermore, the work function of metallic MXenes demonstrates a strong sensitivity to the specific surface termination elements[16,22,23]. For example, oxygen-terminated metallic MXenes exhibit a higher work function compared to their counterparts terminated with fluorine or hydroxyl groups. This tunability of the work function through surface modification provides a powerful tool for engineering the electronic properties of MXenes and optimizing their performance in device applications. The tunable electronic properties of MXenes, ranging from metallic to semiconducting via surface termination, allow for the realization of 2D–2D metal–semiconductor junctions within the same material framework[21,24,25].

Furthermore, the solid-solution approach in MXenes offers a promising pathway for designing alloy-phase-based metal-semiconductor lateral heterointerfaces with intrinsically low contact resistance. Numerous studies have explored 2D lateral contacts between TMD-based metals and semiconductors; however, large lattice mismatch, high Schottky barrier heights, and poor electronic conductivity have limited their suitability for high-performance FET applications[26,27]. An alternative strategy involves phase engineering of MoS$_2$ by converting the semiconducting 2H phase into the metallic 1T phase to form seamless lateral contacts without changing the material's composition. However, such phase transitions inevitably introduce interface defects and dangling bonds, which hinder complete suppression of MIGS[14]. In contrast, our alloy phase engineering approach preserves the same crystal structure across both metallic and semiconducting regions. This strategy, uniquely feasible in MXenes due to their versatile chemical tunability, enables the formation of a coherent and continuous interface. The resulting valency compatibility and minimized electronic discontinuities considerably reduce the formation of MIGS, thereby improving charge injection and interface performance.

This study investigates the potential of M$_2$CT$_2$ MXenes for constructing high-performance 2D-2D metal-semiconductor contacts. We propose an approach leveraging the stability of MXene alloy phases to engineer lateral contacts with low resistivity. By controlling alloy composition, we aim to achieve a seamless transition from metallic to semiconducting behavior within the MXene structure, minimizing the Schottky barrier. We screened 21 M$_2$CT$_2$ MXene compositions using DFT simulations and identified six semiconductors and 15 metals. For each composition, two distinct structural configurations were considered, namely the TT phase with octahedral coordination and the HH phase with trigonal prismatic coordination for transition-metal atoms in both layers. A systematic screening process for optimum semiconductor-metal pair, considering Schottky barrier height and lattice mismatch, identified three promising candidates: Ta$_2$CO$_2$-Ti$_2$CO$_2$, Nb$_2$CO$_2$-Ti$_2$CO$_2$, and Zr$_2$CF$_2$-Sc$_2$CF$_2$. To further assess their potential, we conduct a detailed investigation of the current–voltage (I–V) characteristics of lateral contacts formed with these combinations using the non-equilibrium Green's function (NEGF) method. We further investigated Ta$_{2x}$Ti$_{2(1-x)}$CO$_2$-Ti$_2$CO$_2$ (where $x = 0.25$, 0.5, and 0.75) contacts and demonstrated tunability of contact properties through alloying. This study provides a theoretical foundation for designing MXene-based 2D-2D metal-semiconductor contacts with low contact resistance, highlighting their potential to advance nanoelectronics.

Methods

The structural and electronic properties of MXenes were studied using density functional theory (DFT) with the Vienna *ab initio* simulation package (VASP)[28]. The electron exchange-correlation interaction was approximated using the Perdew-Burke-Ernzerhof (PBE) functional within the generalized gradient approximation (GGA)[29]. To account for the strong on-site Coulombic repulsion effects in transition metals, GGA + U

calculations were employed[30]. A U value of 4 eV was applied for all transition metals, in accordance with typical literature values[31]. The plane wave energy cutoff was set to 400 eV to ensure an accurate depiction of the ground state. The Brillouin zone was sampled with $12 \times 12 \times 1$ k-grid. These parameters were chosen based on a systematic convergence study to ensure an accurate and reliable description of the ground-state properties (Figure. S1). A vacuum layer of 20 Å was introduced to prevent interlayer interactions. All structures were optimized until the changes in total energy and Hellmann-Feynman forces were less than 10^{-6} and 0.01 eV/Å, respectively. Bader charge analysis is employed to quantify the charge transfer from the metal to the semiconductor at the interface[32].

Quantum transport calculations were performed using the NEGF technique within the TranSIESTA code, employing a Double-Zeta Polarized (DZP) basis set[33–35]. An energy cutoff of 200 Ry was set for the real-space grid to accurately evaluate the total energy. The electronic temperature was set to 300 K, and the Brillouin zone was sampled with a dense $100 \times 12 \times 1$ Monkhorst-Pack k-grid for transport calculations.

Results and discussion

To engineer low-resistive MXene-based metal-semiconductor edge contacts, a comprehensive investigation of the electronic properties of M$_2$X MXenes was undertaken. This study focused on 21 M$_2$C MXenes (M = Sc, Ti, Zr, Hf, V, Nb, Ta) with O, F, and OH terminations. Both possible phases were considered for each MXene composition based on crystal field symmetries: the TT phase, where both transition metals have octahedral coordination symmetry, and the HH phase, where both transition metals have trigonal prismatic coordination symmetry (Fig. 1a, b). As detailed in Table. S1, only four out of the 21 compositions are stable in the HH phase, while the remaining compositions favor the TT phase, consistent with previous reports[36,37]. Electronic band structure calculations for the most stable phase of each composition revealed that 15 of the 21 MXenes exhibit metallic behavior, characterized by the absence of a band gap near the Fermi level. The remaining six MXenes (Sc$_2$CO$_2$, Sc$_2$CF$_2$, Sc$_2$C(OH)$_2$, Ti$_2$CO$_2$, Zr$_2$CO$_2$, and Hf$_2$CO$_2$) demonstrate semiconducting properties with band gaps ranging from 0.23 to 2.13 eV. Furthermore, the work function, a critical parameter for determining the Schottky barrier height in metal-semiconductor junctions, was found to be strongly dependent on the surface termination. Specifically, the work function decreases as the termination changes from O to OH, followed by F, indicating the relative ease of electron access from OH-terminated surfaces (Fig. 2a). Finally, the positions of the conduction band minimum (CBM) and valence band maximum (VBM) were determined (Fig. 2b) as these are crucial in dictating charge carrier injection efficiency in metal-semiconductor contacts.

To achieve low-resistive MXene-based FETs, the identification of suitable metal-semiconductor contacts with minimal Schottky barriers and lattice mismatch is needed. The Schottky barrier height, which characterizes the energy barrier for charge carrier injection between a metal and semiconductor, plays a critical role in determining the contact resistance (Fig. 3a). Efficient charge injection requires a low Schottky barrier height, ideally approaching zero for ohmic contact formation. According to the Schottky-Mott rule, the Schottky barrier height is defined as:

$$q\phi_{SB,N} = q\phi_m - q\chi_s, \text{ and } q\phi_{SB,P} = E_g - q(\phi_m - \chi_s), \qquad (1)$$

Where $\phi_{SB,N}$ and $\phi_{SB,P}$ represent, n-type and p-type Schottky barrier heights, respectively. ϕ_m is the work function of the metal, q denotes the charge of the electron, E_g is the band gap of the semiconductor, and χ_s is the electron affinity of the semiconductor.

Given the 15 identified metallic and six semiconducting MXenes, a total of 90 possible metal-semiconductor combinations were considered. A systematic screening pipeline (Fig. 3b) was employed to identify promising candidates. Initially, combinations with a lattice mismatch exceeding 3% were excluded. Subsequently, a stringent criterion of a Schottky barrier height below 0.3 eV, suitable for Schottky barrier field-effect transistor (SB-FET) applications, was imposed. This rigorous selection process yielded

three potential combinations: Ta_2CO_2-Ti_2CO_2, Zr_2CF_2-Sc_2CF_2, and Nb_2CO_2-Ti_2CO_2 exhibiting n-type Schottky barrier heights of 0.04, 0.21, and 0.28 eV, respectively (Fig. 3c).

Recognizing that contact resistance is influenced by multiple factors beyond the Schottky barrier height, including carrier density, carrier transmission probability, and depletion region width, further analysis was conducted. To gain a comprehensive understanding of the electrical characteristics, I-V characteristics were investigated using the NEGF method. A device model was constructed with a scattering region composed of metallic and semiconducting MXenes to study electron transmission at the metal-semiconductor interface (Fig. 4). Here, the left electrode is made of metallic MXene, and the right electrode is made of semiconducting MXene. The transport direction was set along the x-axis, with both the electrodes and scattering regions exhibiting periodicity along the y- and z-axes.
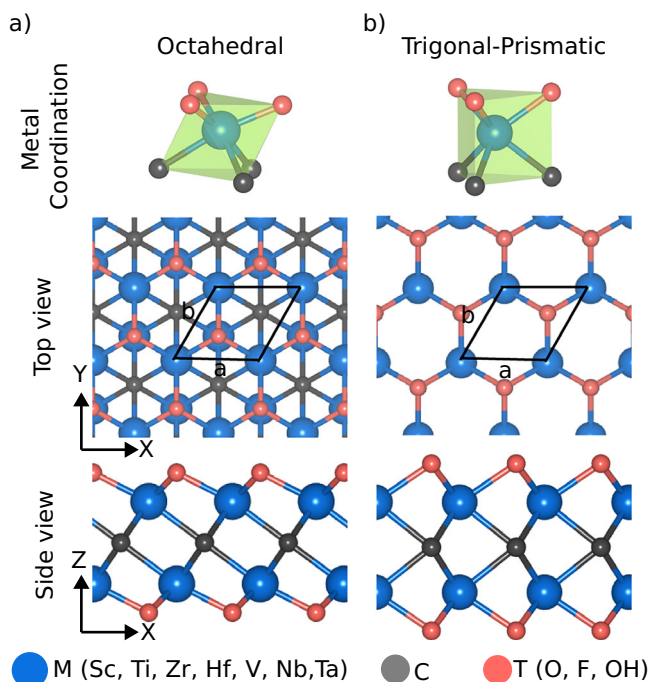
Fig. 1 | Possible phases of M_2CT_2 MXenes based on metal coordination. Schematic representation of metal coordination, top and side views of **a** TT and **b** HH phases in M_2CT_2 MXenes. The black quadrilateral indicates a unit cell.

Importantly, the electrodes were modeled as semi-infinite along the transport direction, while the scattering region remained finite (non-periodic) along the same axis. This model enables a detailed analysis of charge transport across the metal-semiconductor interface.

For the device simulation, a bias voltage ranging from −0.5 to 0.5 V was applied to analyze both n-type and p-type characteristics. To calculate the current (I) we have used the Landaur-Buttiker formula as follows[38]:

$$I(V) = \frac{2e}{\hbar} \int_{-\infty}^{+\infty} T(E, V) \left[f_L(E - \mu_L) - f_R(E - \mu_R) \right] dE, \quad (2)$$

where e is the electronic charge, $\hbar$ is the plank constant, $T(E, V)$ is the transmission function, and μ_L and μ_R are the chemical potential at the left and right electrodes, respectively. The transmission function is determined through the NEGF method, where the system is modeled as a scattering region coupled to two semi-infinite electrodes, and the electron wavefunctions are solved under an applied bias.

The I-V characteristics of the three MXene-based metal-semiconductor lateral contacts, presented in Fig. 5, reveal a non-linear relationship between current and voltage, indicative of Schottky contact behavior. The high ON current in positive biasing religion indicates that all of them are n-type contact. Notably, the Ta_2CO_2-Ti_2CO_2 contact exhibits a considerably higher current compared to the Nb_2CO_2-Ti_2CO_2 and Zr_2CF_2-Sc_2CF_2 contacts. Specifically, the current at 0.5 V for Ta_2CO_2-Ti_2CO_2 contact is 2.2 and 9.37 times higher than Nb_2CO_2-Ti_2CO_2 and Zr_2CF_2-Sc_2CF_2 contacts, respectively. Furthermore, the observed current for all contacts is in the μA range, which is approximately 10^3 times greater than that reported for metal-MoS_2 contact[39,40].

Interestingly, the I–V characteristics of the investigated contacts deviate from the expected Schottky barrier height dependency, suggesting that additional factors contribute to the overall contact resistance. To understand this, the projected local density of states (PLDOS) was calculated for each metal-semiconductor contact, because it provides a real-space representation of the energy alignment between metal and semiconductor states at the interface. As shown in Fig. 6a–c, the Schottky barrier heights after contact formation were determined to be 0.12 eV, 0.24 eV, and 0.29 eV for Ta_2CO_2-Ti_2CO_2, Zr_2CF_2-Sc_2CF_2, and Nb_2CO_2-Ti_2CO_2 respectively. This increase in Schottky barrier height is higher than the value estimated from pristine calculations without contact formation. It arises due to the Fermi-level pinning effect caused by MIGS at the metal-semiconductor interface. All three MXene-based lateral contacts examined in this study exhibit MIGS at the interface (Fig. S2). Furthermore, the carrier density near
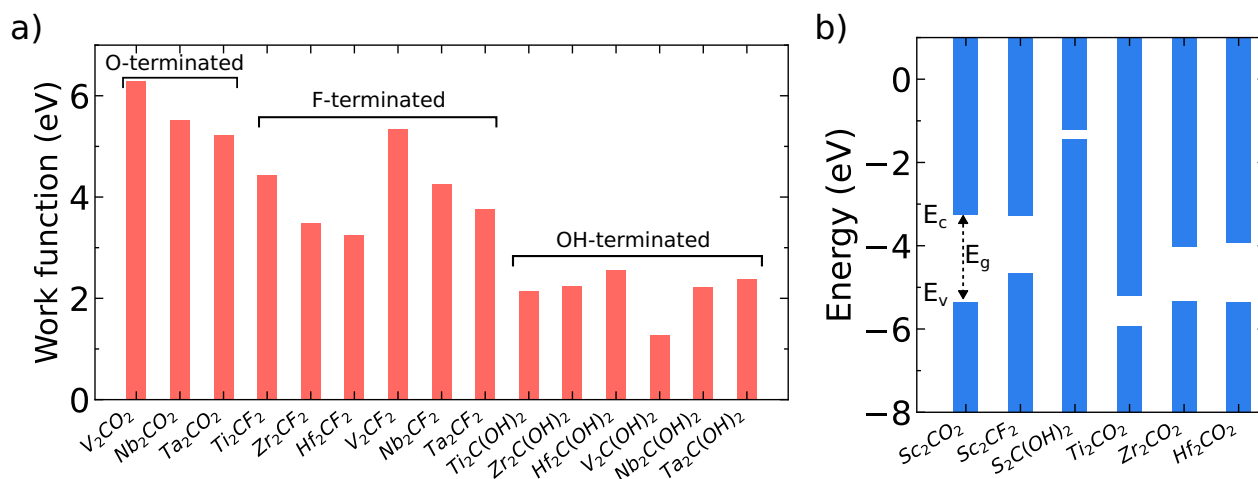

Fig. 2 | Electronic properties of MXenes. a Work function of metallic MXenes. **b** Band alignment of semiconducting MXenes, where E_c, E_v, and E_g represent conduction band minimum (CBM), valence band maximum (VBM), and bandgap energy, respectively.
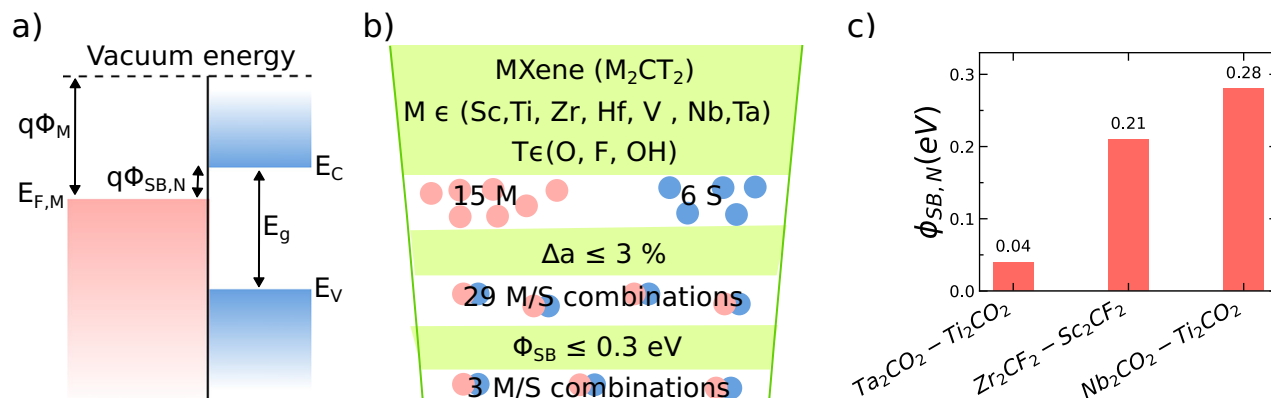
Fig. 3 | Screening metal–semiconductor contacts based on Schottky barrier height and lattice mismatch. a Schematic view of a Schottky junction between a metal and a semiconductor. **b** Schematic representation of computational pipeline to find out the metal–semiconductor combinations with low lattice mismatch and small Schottky barrier height. **c** Calculated n-type Schottky barriers for three metal–semiconductor pairs with lattice mismatch below 3%.
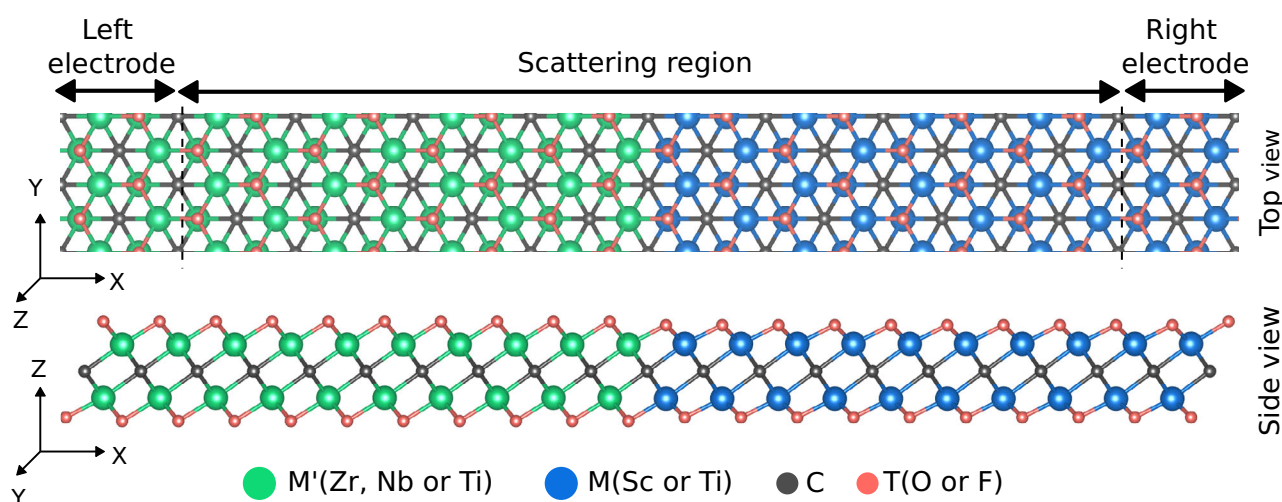
Fig. 4 | Device model for current-voltage characteristics. Top and side views of the M'_2CT_2-M_2CT_2 metal-semiconductor lateral contact device model to study the current-voltage characteristics. In the device structure, the transport direction is set along the x-axis.
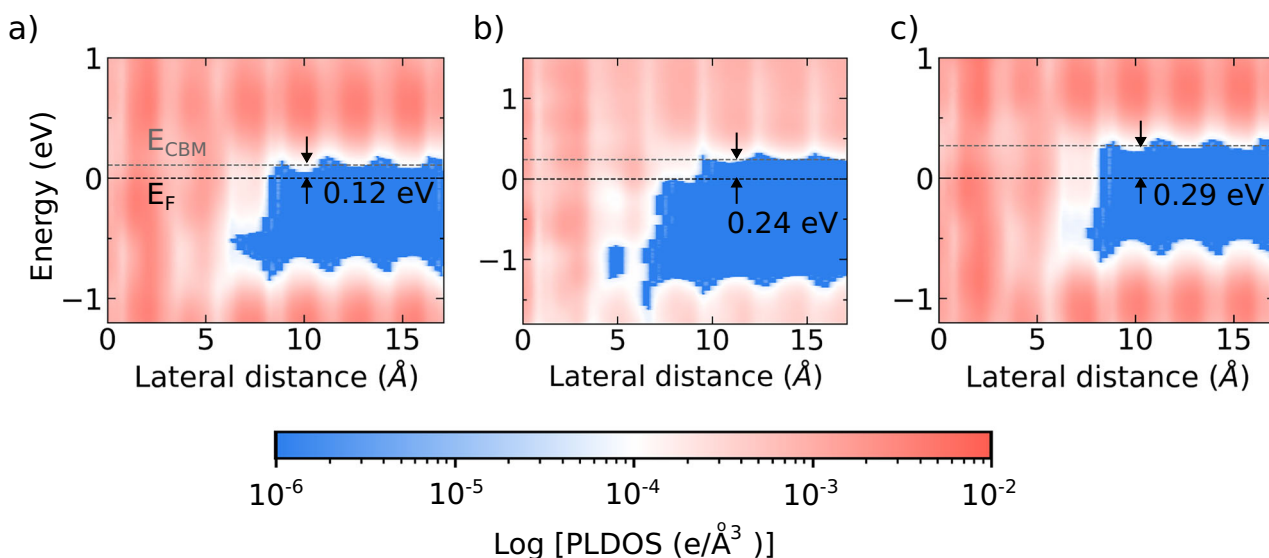
the Fermi level for the Zr_2CF_2-Sc_2CF_2 contact is lower compared to Ta_2CO_2-Ti_2CO_2 and Nb_2CO_2-Ti_2CO_2, as shown in the PLDOS plot (Fig. S2). This behavior arises from the stronger hybridization between O p-orbitals (oxidation state −2) and metal d-orbitals than that between F p-orbitals (oxidation state −1) and metal d-orbitals. Consequently, F-terminated MXenes exhibit a lower density of states near the Fermi level than O-terminated MXenes, resulting in a lower carrier density near the Fermi energy. This reduced carrier density contributes to the lower current observed for the Zr_2CF_2-Sc_2CF_2 contact, despite its lower Schottky barrier height relative to Nb_2CO_2-Ti_2CO_2. Therefore, the overall contact resistance in these MXene-based lateral contacts is governed by two primary factors: the Fermi-level pinning effect induced by MIGS and the charge carrier density near the Fermi level. As carrier density is an intrinsic property of the material, the focus of further optimization lies in mitigating the Fermi-level pinning effect by eliminating MIGS to enhance contact properties. Mitigation of MIGS can be achieved by reducing the electrostatic potential gradient across the metal-semiconductor interface. This objective can be accomplished through the design of alloy phases of metallic MXenes[41].

To this end, alloy phase-engineered metallic MXenes were utilized instead of pristine metallic MXenes in the MXene-based metal-semiconductor contacts. This approach takes advantage of the intrinsic ability of
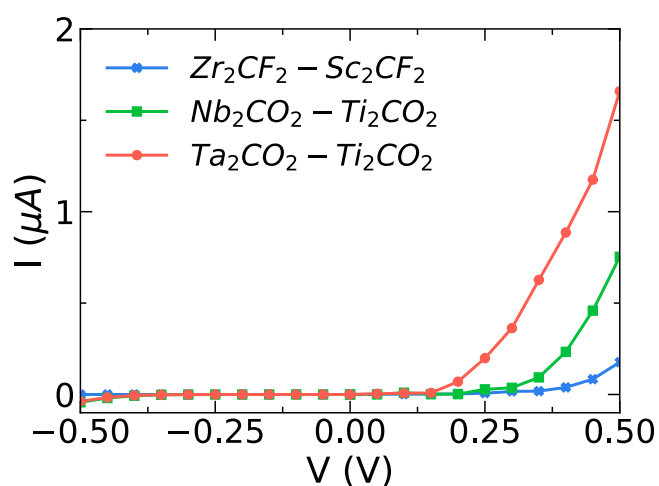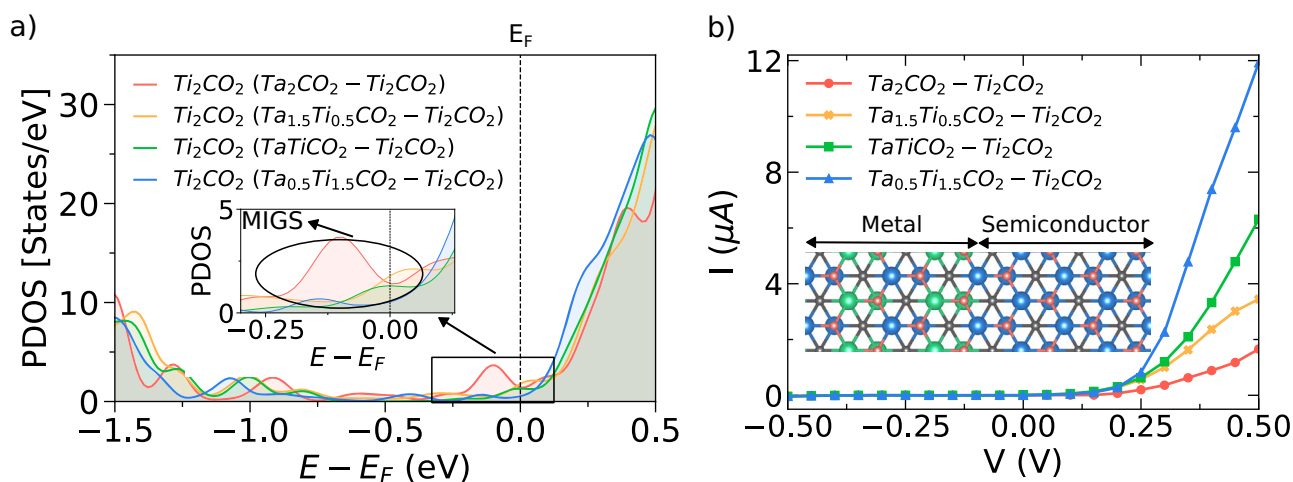

Fig. 5 | Electronic transport in MXene-based lateral contacts. Current-voltage (I–V) characteristic of the model device for three metal-semiconductor lateral contacts with lattice mismatch less than 3% and Schottky barrier height less than 0.3 eV.

Fig. 6 | Projected local density of states (PLDOS) of MXene metal–semiconductor contacts. PLDOS plots for **a** Ta_2CO_2-Ti_2CO_2, **b** Zr_2CF_2-Sc_2CF_2, and **c** Nb_2CO_2-Ti_2CO_2. The Fermi level is set to zero. The black and grey dotted lines represent the Fermi energy (E_F) and conduction band minimum (CBM), respectively.

Fig. 7 | Metal-induced gap states (MIGS) and electronic transport in alloyed MXene-based lateral contacts. a Projected density of states (PDOS) plot for $Ta_{2x}Ti_{2(1-x)}CO_2$-Ti_2CO_2 ($x = 1$, 0.75, 0.5, and 0.25) contacts, showing only the contribution of Ti_2CO_2 to the total density of states (DOS) to identify the MIGS at the interface. Sharp peaks near the Fermi level highlighted in the inset PDOS plot indicate the presence of MIGS at the interface. The Fermi level (E_F) is indicated through dashed lines. **b** Current–voltage (I–V) characteristics of $Ta_{2x}Ti_{2(1-x)}CO_2$-Ti_2CO_2 contacts for varying Ta composition ($x = 1$, 0.75, 0.5, and 0.25). The inset illustrates the schematic representation of the alloy-based metal-semiconductor contact interface used for device modeling.

MXenes to form stable solid solutions, enabling fine-tuning of electronic properties through structural modification. Specifically, for the Ta_2CO_2-Ti_2CO_2 contact, which demonstrated the most efficient I-V characteristics among the shortlisted candidates, an alloy phase with the chemical formula $Ta_{2x}Ti_{2(1-x)}CO_2$ was introduced. The selection of Ti and Ta for alloying was driven by the objective of minimizing both lattice mismatch and electrostatic potential gradient at the interface, thereby effectively reducing the overall contact resistance by mitigating the formation of MIGS. Additionally, the synthesis of the $Ta_{2x}Ti_{2(1-x)}CO_2$-Ti_2CO_2 lateral heterostructure has been recently done by alloying Ti_2CO_2 with varying concentrations of Ta[42–44]. Furthermore, the thermodynamic stability of the three alloy phases considered in this study was evaluated by calculating their formation energies. The results indicate that all alloy phases are thermodynamically stable, with stability increasing progressively as the Ti concentration increases (Table S2).

Subsequently, a device model was constructed with a scattering region composed of alloy phase-engineered metallic and pristine semiconducting MXenes. The I–V characteristics of three alloy MXene-based lateral contacts, $Ta_{2x}Ti_{2(1-x)}CO_2$-Ti_2CO_2 (for $x = 0.25$, 0.5, and 0.75), were investigated. As shown in Fig. 7a, the density of MIGS decreases with decreasing x in $Ta_{2x}Ti_{2(1-x)}CO_2$-Ti_2CO_2 and becomes negligible for the $Ta_{0.5}Ti_{1.5}CO_2$-Ti_2CO_2 contact. Furthermore, Bader charge analysis shows that the amount of charge transferred from the $Ta_{2x}Ti_{2(1-x)}CO_2$ metal contact to the Ti_2CO_2 semiconductor decreases as the Ti content in the alloy increases (Table S3). This decreasing trend suggests that the interfacial dipole becomes weaker with higher Ti concentration. A weaker dipole reduces the extent to which metal wavefunctions penetrate into the semiconductor bandgap, which leads to the suppression of MIGS at the interface. As a result, the Fermi-level pinning effect is reduced, which helps lower the Schottky barrier height and contact resistance. These findings suggest that alloy phase engineering effectively reduces the Fermi-level pinning effect by suppressing MIGS at the metal-semiconductor interface, which is critical for minimizing contact resistance.

The I–V characteristic analysis reveals that all alloy phase-engineered contacts exhibit n-type behavior with considerably higher ON currents

compared to the Ta_2CO_2-Ti_2CO_2 contact (Fig. 7b). For example, the output current at 0.5 V is nearly 7 times higher for $Ta_{0.5}Ti_{1.5}CO_2$-Ti_2CO_2 than for Ta_2CO_2-Ti_2CO_2. Additionally, the slope of the I-V curve within the bias range of 0 to 0.5 V increases with a decrease in x and reaches its maximum for the $Ta_{0.5}Ti_{1.5}CO_2$-Ti_2CO_2 contact, further corroborating the reduction in Schottky barrier height. Overall, these results highlight alloy phase engineering as an effective strategy to reduce the contact resistance of FET devices with MXene-based 2D-2D lateral metal-semiconductor contacts. By suppressing detrimental MIGS and optimizing charge transport across the interface, alloy phase engineering enables the realization of high-performance MXene-based electronics, thereby paving the way for advancements in next-generation FET devices.

Although our results demonstrate a notable enhancement in the $I-V$ characteristics of MXene-based metal-semiconductor contacts via alloy phase engineering, the performance of 2D lateral metal-semiconductor heterocontacts is highly sensitive to interface quality. In experimental settings, interface defects frequently induce metal-induced gap states (MIGS), which pin the Fermi level and result in elevated contact resistance. For instance, the experimentally measured output current in 1T-MoS_2/2H-MoS_2 contacts has been reported to be more than an order of magnitude lower than predictions from NEGF simulations[45]. However, no experimental studies are currently available for direct comparison with our simulation results. Taking into account the influence of interface imperfections, we acknowledge that our theoretical predictions may not quantitatively match future experimental data. Nonetheless, we believe our theoretical framework provides valuable insights and a predictive foundation for the rational design of MXene-based contact architectures, which can guide and inform future experimental efforts.

In addition to interface defects, surface terminations present another critical factor that can influence contact performance in experimental realizations of MXene-based devices. While our simulations predict low contact resistance, the presence of mixed terminations in experimentally synthesized MXenes can considerably alter the contact properties. Given that the work function of MXenes is highly sensitive to the type and distribution of surface terminations, these mixed terminations can increase the Schottky barrier height, thereby contributing to higher contact resistance. To address this challenge, considerable advances have been made in controlling surface chemistry through refined synthesis techniques. For example, low-pressure flash annealing promotes O-rich surface formation, while low-temperature anhydrous etching facilitates F-rich terminations[46,47]. Both methods offer atomic-level precision and reproducibility in surface functionalization. These developments open up new opportunities for tailoring MXene surfaces to meet the specific demands of electronic applications, establishing termination engineering as a powerful strategy for optimizing device performance.

Furthermore, the synthesis of stable MXene alloy phases with specific transition metal ratios is a key requirement for fabricating the proposed alloy-based contact interfaces. Although previous studies have demonstrated the successful synthesis of $Ti_{2x}V_{2(1-x)}AlC$ solid solution MAX phases, the phase stability for a particular Ti/V ratio has been shown to be highly sensitive to the growth temperature[48]. Additionally, Monte Carlo simulations by Wong et al. revealed that the stability of $Ta_{2x}Ti_{2(1-x)}CO_2$ MXenes is strongly dependent on both composition and temperature, indicating a narrow processing window where the alloy remains stable[44]. Based on these findings, it can be inferred that the synthesis of MXene alloy phases with specific Ti/Ta ratios is feasible through careful optimization of growth conditions, particularly temperature.

Moreover, integrating these MXene-based contacts into complementary metal-oxide-semiconductor (CMOS) technology also presents challenges, especially in terms of fabrication processes. Still, the proposed MXene-based lateral heterocontacts offer several advantages for CMOS scaling, such as their ultra-thin structure, tunable work function, and reduced Fermi-level pinning, features that align well with the requirements set by the International Roadmap for Devices and Systems (IDRS). Recent studies have also shown that $Ti_3C_2T_x$ MXenes can be patterned directly onto MoS_2 channels for building 2D FETs[49]. In related work, Jeon et al. demonstrated very low contact resistance in Mo_2C/MoS_2 lateral heterocontacts and provided a detailed analysis of the resulting transistor behavior[50]. These findings support the feasibility of using alloy-engineered MXene contacts in CMOS-compatible electronic devices.

Conclusions

This study presents a comprehensive investigation of MXene-based metal-semiconductor contacts for the development of high-performance FETs, aligning with the increasing demand for downscaling of transistors as outlined in the IDRS requirements. MXenes, with their unique combination of metallic conductivity and tunable electronic properties, hold immense promise for next-generation electronics. This study leverages these attributes to engineer high-performance metal-semiconductor contacts for future MXene-based FETs. By employing a comprehensive design approach encompassing first-principles calculations, transport simulations, and alloy phase engineering, we demonstrate the feasibility of achieving low-resistance contacts with high current-carrying capacity.

We exploit the diverse chemistry of MXenes to screen for optimal metal-semiconductor combinations based on criteria of minimal lattice mismatch and low Schottky barrier height. This strategy, coupled with a detailed analysis of the electronic structure and charge transport, led to the identification of the Ta_2CO_2–Ti_2CO_2 heterojunction as a promising candidate. Notably, this contact exhibits a remarkably low Schottky barrier height of 0.04 eV and high current density. Subsequent analysis of the $I-V$ characteristics, obtained using NEGF formalism, revealed the critical role of carrier density near the Fermi level and the detrimental impact of MIGS. To mitigate these effects, we introduce an alloying strategy, forming a $Ta_{2x}Ti_{2(1-x)}CO_2$-Ti_2CO_2 solid solution at the interface. This approach effectively suppresses MIGS formation and enhances charge transport, further improving the electrical characteristics.

This research underscores the potential of MXenes as building blocks for next-generation electronic devices. The combination of their unique electronic properties, diverse chemical compositions, and amenability to alloying provides a versatile platform for tailoring metal-semiconductor contacts. The findings presented here not only advance the fundamental understanding of charge transport in MXene heterojunctions but also offer a practical pathway for engineering low-resistance contacts in future MXene-based FETs, ultimately contributing to the downscaling of transistors. Future research directions include exploring the performance of these MXene-based contacts in actual device architectures, investigating the influence of different dielectric environments, and extending the alloying strategy to other MXene combinations. Moreover, the insights gained from this study can inform the design and optimization of MXene-based heterojunctions for a broader range of electronic applications, including sensors and optoelectronics.

Data availability

All relevant data have been included in the manuscript and supplementary information. Any additional data that support the findings of this study are available from the corresponding author upon reasonable request.

References

1. Waldrop, M. M. The chips are down for Moore's law. *Nat. News* **530**, 144 (2016).
2. Liu, Y. et al. Promises and prospects of two-dimensional transistors. *Nature* **591**, 43–53 (2021).
3. Chhowalla, M., Jena, D. & Zhang, H. Two-dimensional semiconductors for transistors. *Nat. Rev. Mater.* **1**, 1–15 (2016).
4. Liu, Y., Duan, X., Huang, Y. & Duan, X. Two-dimensional transistors beyond graphene and TMDCs. *Chem. Soc. Rev.* **47**, 6388–6409 (2018).

5. Radisavljevic, B., Radenovic, A., Brivio, J., Giacometti, V. & Kis, A. Single-layer MoS2 transistors. *Nat. Nanotechnol.* **6**, 147–150 (2011).

6. Liu, H., Neal, A. T. & Ye, P. D. Channel length scaling of MoS2 MOSFETs. *ACS Nano* **6**, 8563–8569 (2012).

7. Li, L. et al. Black phosphorus field-effect transistors. *Nat. Nanotechnol.* **9**, 372–377 (2014).

8. Tao, L. et al. Silicene field-effect transistors operating at room temperature. *Nat. Nanotechnol.* **10**, 227–231 (2015).

9. Madhushankar, B. et al. Electronic properties of germanane field-effect transistors. *2D Mater* **4**, 021009 (2017).

10. Liu, Y. et al. Approaching the Schottky–Mott limit in van der Waals metal–semiconductor junctions. *Nature* **557**, 696–700 (2018).

11. Kang, J., Liu, W., Sarkar, D., Jena, D. & Banerjee, K. Computational study of metal contacts to monolayer transition-metal dichalcogenide semiconductors. *Phys. Rev. X* **4**, 031005 (2014).

12. Tung, R. T. Chemical bonding and Fermi level pinning at metal-semiconductor interfaces. *Phys. Rev. Lett.* **84**, 6078 (2000).

13. Kim, C. et al. Fermi level pinning at electrical metal contacts of monolayer molybdenum dichalcogenides. *ACS Nano* **11**, 1588–1596 (2017).

14. Kappera, R. et al. Phase-engineered low-resistance contacts for ultrathin MoS2 transistors. *Nat. Mater.* **13**, 1128–1134 (2014).

15. Khazaei, M., Ranjbar, A., Arai, M., Sasaki, T. & Yunoki, S. Electronic properties and applications of MXenes: a theoretical review. *J. Mater. Chem. C* **5**, 2488–2503 (2017).

16. Schultz, T. et al. Surface termination dependent work function and electronic properties of Ti3C2T x MXene. *Chem. Mater.* **31**, 6590–6597 (2019).

17. Hart, J. L. et al. Control of MXenes' electronic properties through termination and intercalation. *Nat. Commun.* **10**, 522 (2019).

18. Zha, X.-H. et al. Promising electron mobility and high thermal conductivity in Sc 2 CT 2 (T = F, OH) MXenes. *Nanoscale* **8**, 6110–6117 (2016).

19. Shahzad, F., Iqbal, A., Kim, H. & Koo, C. M. 2D transition metal carbides (MXenes): applications as an electrically conducting material. *Adv. Mater.* **32**, 2002159 (2020).

20. Khazaei, M. et al. Nearly free electron states in MXenes. *Phys. Rev. B* **93**, 205125 (2016).

21. Hantanasirisakul, K. & Gogotsi, Y. Electronic and optical properties of 2D transition metal carbides and nitrides (MXenes). *Adv. Mater.* **30**, 1804779 (2018).

22. Koh, S. W. et al. Tuning the work function of MXene via surface functionalization. *ACS Appl. Mater. Interfaces* **49**, 66826–66836 (2023).

23. Khazaei, M. et al. OH-terminated two-dimensional transition metal carbides and nitrides as ultralow work function materials. *Phys. Rev. B* **92**, 075411 (2015).

24. Mozafari, M. & Soroush, M. Surface functionalization of MXenes. *Mater. Adv.* **2**, 7277–7307 (2021).

25. Anasori, B. et al. Control of electronic properties of 2D carbides (MXenes) by manipulating their transition metal layers. *Nanoscale Horiz.* **1**, 227–234 (2016).

26. Wang, Z. et al. Substitutional p-type doping in NbS2–MoS2 lateral heterostructures grown by MOCVD. *Adv. Mater.* **35**, 2209371 (2023).

27. Song, S. et al. Atomic transistors based on seamless lateral metal-semiconductor junctions with a sub-1-nm transfer length. *Nat. Commun.* **13**, 4916 (2022).

28. Kresse, G. & Furthmüller, J. Efficient iterative schemes for ab initio total-energy calculations using a plane-wave basis set. *Phys. Rev. B* **54**, 11169 (1996).

29. Perdew, J. P., Burke, K. & Ernzerhof, M. Generalized gradient approximation made simple. *Phys. Rev. Lett.* **77**, 3865 (1996).

30. Dudarev, S., Botton, G., Savrasov, S., Humphreys, C. & Sutton, A. Electron-energy-loss spectra and the structural stability of nickel oxide: An LSDA + U study. *Phys. Rev. B* **57**, 1505 (1998).

31. Dong, L., Kumar, H., Anasori, B., Gogotsi, Y. & Shenoy, V. B. Rational design of two-dimensional metallic and semiconducting spintronic materials based on ordered double-transition-metal MXenes. *J. Phys. Chem. Lett.* **8**, 422–428 (2017).

32. Sanville, E., Kenny, S. D., Smith, R. & Henkelman, G. Improved grid-based algorithm for Bader charge allocation. *J. Comput. Chem.* **28**, 899–908 (2007).

33. Datta, S. Nanoscale device modeling: the Green's function method. *Superlattices Microstruct.* **28**, 253–278 (2000).

34. Brandbyge, M., Mozos, J.-L., Ordejón, P., Taylor, J. & Stokbro, K. Density-functional method for nonequilibrium electron transport. *Phys. Rev. B* **65**, 165401 (2002).

35. Papior, N., Lorente, N., Frederiksen, T., García, A. & Brandbyge, M. Improvements on non-equilibrium and transport Green function techniques: The next-generation transiesta. *Comput. Phys. Commun.* **212**, 8–24 (2017).

36. Bera, S. & Kumar, H. Phase stability of MXenes: understanding the role of coordination symmetries, transition metals, and surface terminations. *J. Phys. Chem. C* **127**, 20734–20741 (2023).

37. Gouveia, J. D., Viñes, F., Illas, F. & Gomes, J. R. MXenes atomic layer stacking phase transitions and their chemical activity consequences. *Phys. Rev. Mater.* **4**, 054003 (2020).

38. Landauer, R. Electrical resistance of disordered one-dimensional lattices. *Philos. Mag.* **21**, 863–867 (1970).

39. Late, D. J., Liu, B., Matte, H. R., Dravid, V. P. & Rao, C. Hysteresis in single-layer MoS2 field effect transistors. *ACS Nano* **6**, 5635–5641 (2012).

40. Pal, A. et al. Characterization and closed-form modeling of edge/top/hybrid metal-2D semiconductor contacts. In *Proc. 2022 International Electron Devices Meeting (IEDM)* 28–5 (IEEE, 2022).

41. Li, X. et al. Two-dimensional metallic alloy contacts with composition-tunable work functions. *Nat. Electron.* **6**, 842–851 (2023).

42. Wong, Z. M., Tan, T. L., Tieu, A. J. K., Yang, S.-W. & Xu, G. Q. Computational discovery of transparent conducting in-plane ordered MXene (i-MXene) alloys. *Chem. Mater.* **31**, 4124–4132 (2019).

43. Tan, T. L., Jin, H. M., Sullivan, M. B., Anasori, B. & Gogotsi, Y. High-throughput survey of ordering configurations in MXene alloys across compositions and temperatures. *ACS Nano* **11**, 4407–4418 (2017).

44. Wong, Z. M., Tan, T. L., Yang, S.-W. & Xu, G. Q. Enhancing the photocatalytic performance of MXenes via stoichiometry engineering of their electronic and optical properties. *ACS Appl. Mater. Interfaces* **10**, 39879–39889 (2018).

45. Nourbakhsh, A. et al. MoS2 field-effect transistor with sub-10 nm channel length. *Nano Lett* **16**, 7798–7806 (2016).

46. Zhao, Y. et al. Anhydrous organic etching derived fluorine-rich terminated MXene nanosheets for efficient and stable perovskite solar cells. *Chem. Eng. J.* **469**, 143862 (2023).

47. Yin, S.-H. et al. A general method for precise modification of–O termination on MXenes by low-pressure flash annealing. *J. Mater. Chem. A* **13**, 15725–15735 (2025).

48. Simonenko, E. et al. Synthesis of MAX phases in the Ti2AlC–V2AlC system as precursors of heterometallic MXenes Ti2–x V x C. *Russ. J. Inorg. Chem.* **67**, 705–714 (2022).

49. Xu, X. et al. High-yield Ti3C2Tx MXene–MoS2 integrated circuits. *Adv. Mater.* **34**, 2107370 (2022).

50. Jeon, J. et al. Epitaxial synthesis of molybdenum carbide and formation of a Mo2C/MoS2 hybrid structure via chemical conversion of molybdenum disulfide. *ACS Nano* **12**, 338–346 (2018).

Acknowledgements

Author contributions

S.B. and H.K. were responsible for the methodology, conceptualization, visualization, and drafting of the initial manuscript. D.K. contributed to the analysis of results.

Competing interests

The authors declare no competing interests.

Additional information